Applied Physics Letters

RESEARCH ARTICLE | APRIL 02 2025

Low crosstalk modular flip-chip architecture for coupled superconducting qubits

Special Collection: Quantum Networks

Soeren Ihssen; Simon Geisert; Gabriel Jauma; Patrick Winkel; Martin Spiecker; Nicolas Zapata; Nicolas Gosling; Patrick Paluch; Manuel Pino; Thomas Reisinger; Wolfgang Wernsdorfer; Juan Jose Garcia-Ripoll; Ioan M. Pop

Appl. Phys. Lett. 126, 134003 (2025)
https://doi.org/10.1063/5.0245667

Applied Physics Letters ARTICLE pubs.aip.org/aip/apl

Low crosstalk modular flip-chip architecture for coupled superconducting qubits

Cite as: Appl. Phys. Lett. **126**, 134003 (2025); doi: 10.1063/5.0245667
Submitted: 28 October 2024 · Accepted: 4 March 2025 ·
Published Online: 2 April 2025

Soeren Ihssen,[1] Simon Geisert,[1] Gabriel Jauma,[2,3] Patrick Winkel,[1,4,5] Martin Spiecker,[1] Nicolas Zapata,[1] Nicolas Gosling,[1] Patrick Paluch,[1,6] Manuel Pino,[2,7] Thomas Reisinger,[1] Wolfgang Wernsdorfer,[1,6] Juan Jose Garcia-Ripoll,[2] and Ioan M. Pop[1,6,8,a)]

AFFILIATIONS

[1]IQMT, Karlsruhe Institute of Technology, 76131 Karlsruhe, Germany
[2]Institute of Fundamental Physics IFF-CSIC, Calle Serrano 113b, 28006 Madrid, Spain
[3]Applied Physics Department, Salamanca University, Salamanca 37008, Spain
[4]Departments of Applied Physics and Physics, Yale University, New Haven, Connecticut 06520, USA
[5]Yale Quantum Institute, Yale University, New Haven, Connecticut 06520, USA
[6]PHI, Karlsruhe Institute of Technology, 76131 Karlsruhe, Germany
[7]Nanotechnology Group, USAL-Nanolab, Salamanca University, Salamanca 37008, Spain
[8]Physics Institute 1, Stuttgart University, 70569 Stuttgart, Germany

Note: This paper is part of the APL Special Topic, Quantum Networks.
[a)]**Author to whom correspondence should be addressed:** ioan.pop@kit.edu

ABSTRACT

We present a flip-chip architecture for an array of coupled superconducting qubits, in which circuit components reside inside individual microwave enclosures. In contrast to other flip-chip approaches, the qubit chips in our architecture are electrically floating, which guarantees a simple, fully modular assembly of capacitively coupled circuit components, such as qubit, control, and coupling structures as well as reduced crosstalk between the components. We validate the concept with a chain of three nearest neighbor coupled generalized flux qubits in which the center qubit acts as a frequency-tunable coupler. Using this coupler, we demonstrate a transverse coupling on/off ratio ≈ 50, $zz-$crosstalk ≈ 0.7 kHz between resonant qubits and isolation between the qubit enclosures > 60 dB.

Circuit quantum electrodynamics[1]—using superconducting qubits, resonators, and waveguides as building blocks—is one of the leading platforms for quantum hardware development. Following an approach similar to the semiconductor industry, the on-chip integration of an increasing number of such components is, in principle, a matter of sophisticated engineering, and it has led to the realization of impressively complex quantum processors.[2–8] However, as quantum processors grow in size and complexity, new physical phenomena emerge, such as correlated quasiparticle and phonon bursts,[9,10] charge offsets,[11] and two-level-system reconfigurations due to ionizing radiation.[12,13] Moreover, microwave crosstalk emerges as one of the main limitations in some of the most sophisticated architectures.[8] Last, but not least, it becomes increasingly likely that frequency crowding or a single defective component limits the performance of an entire chip. In view of these challenges, it is essential for scale-up strategies to minimize microwave and mechanical (i.e., phonon) crosstalk and maximize modularity.

On-chip strategies to scale-up quantum processors include from a technological perspective relatively involved techniques such as air-bridges,[14] spring-loaded pogo pins,[15] or deep silicon vias.[16] While these monolithic devices can achieve impressive microwave performance in terms of isolation and spurious mode suppression, they are susceptible to correlated phonon bursts and lack modularity due to cold-welded connections between layers. A complementary approach is to assemble a processor from chip-level building blocks, allowing for individual component fabrication as well as flexible and reconfigurable arrangements. Several promising techniques are currently being pursued,[17–20] including flip-chip[21,22] and chiplet[23–25] architectures.

Here, we present an alternative modular approach, where we combine several features of 2D and 3D architectures to form an array of coupled, but crosstalk-resilient superconducting qubits. Our goal is to facilitate a highly modular assembly, with microwave-isolated subcomponents insensitive to correlated errors caused by the propagation of phonon waves. The key feature in our design is the separation of the qubits on dedicated, electrically floating chips within individual microwave enclosures. To validate the architecture, we implemented a device consisting of three enclosures, each hosting a generalized flux qubit (Q), inductively coupled to a dedicated readout (R) mode referred to as QR system, similar to Ref. 26. We use the central qubit as a flux-tunable coupler and demonstrate tunable two-qubit interactions. This concept can be extended by adding microwave enclosures, both in-plane and out-of-plane, to increase the number of adjacent qubits.

The three enclosures of our prototype, each hosting a QR system on a dedicated chip, are shown in Fig. 1(a). They have dimensions of $6.1 \times 6.1 \times 6.0\,\mathrm{mm}^3$, pushing the enclosures lowest frequency eigenmodes above 16 GHz. The 6.5 mm spacing between neighboring qubits facilitates their assembly without the need for sophisticated packaging tools and strongly reduces crosstalk. In the outer enclosures on the left and right [e1 and e3, respectively, see Fig. 1(b)], we mount an upside-down flipped qubit chip on top of a control chip, while the middle enclosure (e2) contains only a single coupler chip. The qubit chip dimensions ($2.85 \times 10.0\,\mathrm{mm}^2$) exceed the size of their enclosures, so that they overlap with the adjacent enclosures. We attach the top qubit chips with a small amount of vacuum grease to pedestals

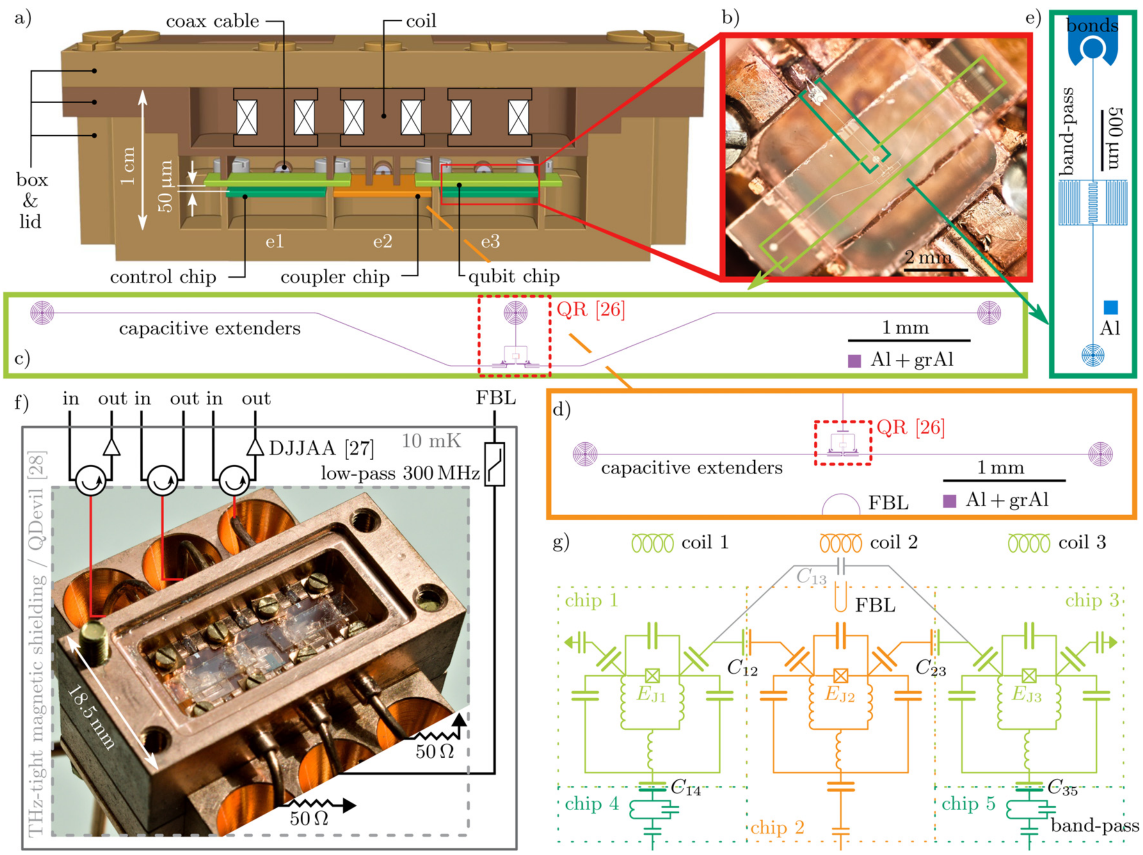

FIG. 1. Modular flip-chip architecture based on individual qubit and coupler enclosures. (a) Cross section of the sample box: two of the three enclosures (e1 and e3) contain control (dark green) and qubit (light green) chips, one enclosure (e2) houses a qubit chip used as coupler (orange). Each enclosure can be accessed by two coaxial cables perpendicular to the cross section plane, one on each side. The static magnetic field in each enclosure is controlled by coils integrated in the top lid, which are highlighted via the black X symbols. (b) Optical image of the qubit-chip above the control chip in e1, without a coupler chip present. (c)–(e) Design layouts of the qubit, coupler, and control chips, respectively. The QR system consists of a generalized flux qubit inductively coupled to a readout resonator, as described in Ref. 26. The QR system is indicated by the red frames in panels (c) and (d). Two capacitive extenders are capacitively coupled to the qubit junction electrodes to enable capacitive coupling to the adjacent chips via the skeletal shaped pads. The middle pad in panel (c) is used to couple the QR system to the input–output control chip shown in panel (e). The bandpass filter implemented by the meandered inductor and finger capacitor visible in the center of the chip in panel (d) is used to reduce Purcell decay.[27,28] Through pulses on the flux bias line (FBL) visible in panel (d), the frequency of the coupler qubit is tunable. The color legend indicates the material used for each circuit element: blue for aluminum (Al) and purple for Al covered with granular aluminum (grAl). (f) Optical image of the fully equipped sample box and schematics of the reflection measurement setup in a magnetically shielded environment at 10 mK. The FBL is connected to a bulk commercial low-pass filter with a cutoff frequency of 300 MHz. (g) Circuit diagram of the coupled qubit array. Each qubit chip (chips 1 and 3) contains a QR system[26] with a corresponding bandpass filter [cf. panel (d)] on its control chip (chips 4 and 5, respectively). The QR used as coupler is located on-chip 2. The coupling capacitances C_{12}, C_{23}, C_{14}, and C_{35} bridge the gaps between individual chips, enabling a modular flip-chip architecture. The capacitance C_{13} is not implemented on the chips and represents the direct capacitive coupling between the outer qubits.

inside the enclosures. We fix the bottom chips with titanium or copper screws to the sample box and wire bond to the coaxial ports. The pedestals define the $d = 50 \pm 10\ \mu$m gap between the top and bottom chips, avoiding cold-welded bump bonds or on-chip spacers. The qubit chips contain a QR system, as described in Ref. 26, to which we add capacitive extenders that reach into the adjacent enclosures [see Figs. 1(b) and 1(c)]. The pads at the end of the extenders and in the center of the chips are used for capacitive coupling across the gap between the chips, which is discussed in more detail in the supplementary material. We chose a skeletal pattern for the pads to avoid flux trapping. The coupler chip in e2 also houses a QR system connected via capacitive extenders to pads [see Fig. 1(d)], aligned with the corresponding neighboring qubits' coupling pads. Details of the fabrication can be found in the supplementary material.

The control chips below each qubit chip in e1 and e3 accommodate a bond pad, capacitively coupled to a bandpass filter, which is connected to a capacitive pad in the center of the qubit chip [see Fig. 1(e)]. The bandpass filter reduces Purcell decay[27,28] and enables the coupling of the readout mode to the coaxial input port (see the supplementary material). The control structures for the coupler, which consist of a fast flux bias line (FBL) and a readout line as shown in Fig. 1(d), are on the same chip. The FBL on the center coupler chip is wire-bonded to a coaxial cable, which is equipped with a 300 MHz low-pass filter.

The picture in Fig. 1(f) shows an open sample box made of copper, and it provides an overview of the entire assembly of five chips, which is further enclosed in a magnetic shield[29] and thermally anchored to the baseplate of a dilution cryostat. We show an equivalent circuit diagram of the assembly in Fig. 1(g). Note that the three individual enclosures are defined by the lid, which is not visible in the picture. The simplified schematics of the microwave readout and control lines are also shown in Fig. 1(f). We perform individual qubit readout by probing the readout resonators on the qubit chips in reflection. We use dimer Josephson junction array parametric amplifiers (DJJAAs)[30] for the readout of the two qubits in e1 and e3. Qubit control pulses are also send through the readout lines. Simultaneous readout and single qubit π-pulse calibration measurement are shown in the supplementary material.

We show the measured two-tone spectroscopy for the qubits and coupler close to their half-flux points (i.e., the magnetic flux sweet spots) in Fig. 2. Their frequencies can be tuned independently via the three magnetic field coils, after calibrating the static magnetic field crosstalks. To operate the device, we define the idle points to be the sweet spots of qubit 1 and coupler, which are at $f_{q1} = 3.689$ GHz and $f_c = 3.437$ GHz, respectively. Exploiting the fact that the qubits are isolated in distant enclosures, we chose to operate qubits 1 and 3 on resonance. To turn on coupling between qubits 1 and 3, we play fast flux pulses on the FBL to tune the coupler closer to the qubits 1 and 3 bias points.

In view of the fact that we operate the qubits on resonance, it is paramount to know the isolation and crosstalk between the enclosures when the coupling is turned off. Figure 3(a) illustrates schematically the crosstalk present in our system. To identify the port-to-resonator isolation, we drive resonator 1 ($f_{r1} = 6.508$ GHz) and resonator 3 ($f_{r3} = 5.226$ GHz) through the readout port of e3. We measure readout-induced dephasing for both qubits via Ramsey interferometry vs drive power and drive frequency and fit it to a dispersive model,[31] detailed in the supplementary material. We extract the isolation between enclosures from the ratio of power transmission coefficients. Fitting the measured data shown in Fig. 3, we obtain an isolation of 64 ± 0.5 dB.

To test qubit control crosstalk, we drive via port 3 and measure Rabi oscillations vs drive amplitude on both qubits for a 1 μs long pulse. We fit the linear dependence of the measured Rabi frequencies Ω_i with applied drive amplitude, as shown in Fig. 3(c). Following Refs. 20 and 32, we extract a port-to-qubit crosstalk, also known as qubit drive selectivity, of

$$10 \log_{10}\left(\frac{\Omega_1}{\Omega_3}\right)^2 \approx -60\ \text{dB}, \tag{1}$$

which allows to drive simultaneous Rabi oscillations of qubit 1 and qubit 3 on resonance ($f_{q1} = f_{q3}$) with less than 1‰ crosstalk error.

We quantify the longitudinal interaction between qubits 1 and 3 by measuring Ramsey fringes on qubit 1, with and without playing a

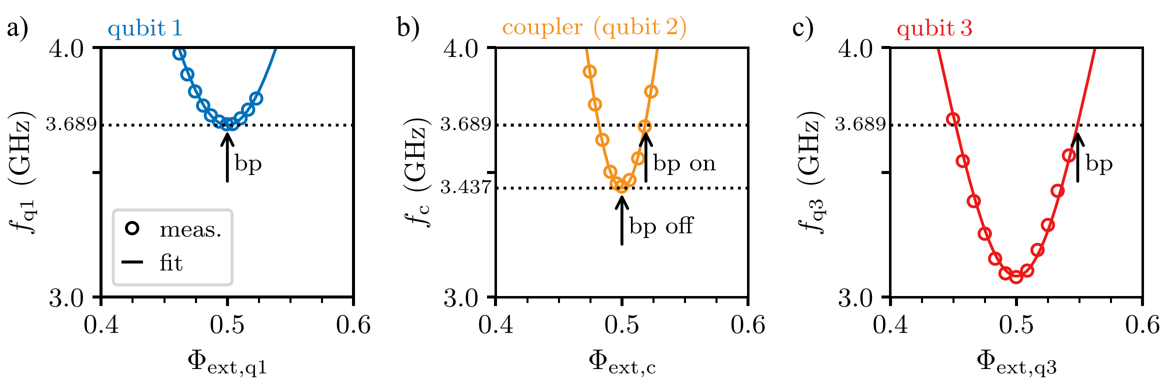

FIG. 2. Overview of qubit and coupler spectra with bias points (bp). The measured (circles) and fitted (lines) spectra of (a) qubit 1 (q1, blue) in e1, (b) the coupler (c, orange)—i.e., qubit 2—in e2, and (c) qubit 3 (q3, red) in e3 vs the external flux Φ_{ext} through the respective qubit/coupler loops are shown. During all experiments, both qubits (q1 and q3) are operated at a frequency of $f_{q1} \approx f_{q3} \approx 3.689$ GHz [see the corresponding bp in panels (a) and (c)], corresponding to the half-flux point of q1 ($\Phi_{ext,q1} = \Phi_0/2$). To switch the coupler off, coil 2 is used to park the coupler at its half-flux point ($\Phi_{ext,c} = \Phi_0/2$), corresponding to bp off at a frequency of 3.437 GHz. To switch the coupler on, a DC pulse is played on the FBL, aligning f_c at bp on, resonant with f_{q1} and f_{q3}.

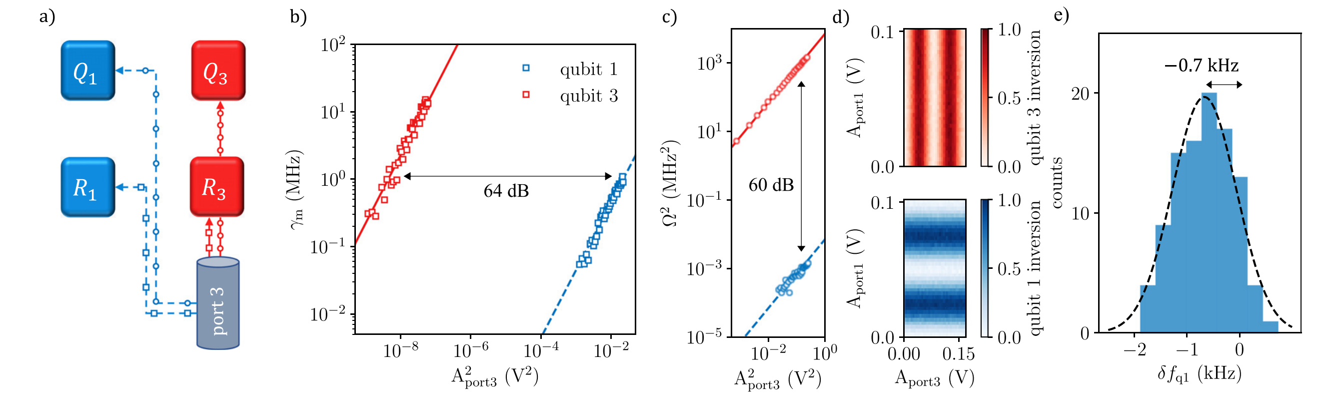

FIG. 3. Isolation and crosstalk with coupler switched off. (a) Sketch of the microwave crosstalk measurement scheme: qubit 3 and resonator 3 are driven via microwave signals applied at port 3 (solid red lines). Port-to-qubit and port-to-resonator crosstalk affects qubit 1 and resonator 1 when driving on resonance through port 3 (dashed blue lines). (b) Measurement-induced dephasing rate γ_m of qubit 1 (blue) and qubit 3 (red), vs power at port 3. The dephasing rate is extracted from damped Ramsey fringes and fitted to a dispersive model, see the supplementary material. We measure an isolation between enclosures 1 and 3 of 64±0.5 dB. The black arrow is a qualitative guide to the eye. (c) Rabi frequencies Ω of qubit 1 (blue) and qubit 3 (red) extracted from Rabi oscillations induced by driving at port 3. The measured port-to-qubit isolation is 60 dB. (d) Simultaneous driving of qubits 1 and 3 biased on resonance ($f_{q1} = f_{q3} = 3.689$ GHz) with the coupler switched off ($f_c = 3.437$ GHz). The x- and y-axis depict the drive amplitudes at port 1 and port 3, respectively. The qubits can be manipulated independently while being on resonance. (e) Measured zz-crosstalk between qubit 1 and qubit 3. We extract δf_{q1} from the difference of Ramsey fringe frequency of qubit 1 when the qubit 3 population is inverted. From a Gaussian fit to the measured δf_{q1} histogram we extract $\delta\bar{f}_{q1} = -0.7 \pm 0.5$ kHz.

π-pulse on qubit 3. The measured shifts in qubit 1 frequencies, δf_{q1}, are summarized in Fig. 3(d). The resulting zz-crosstalk is described by a Gaussian distribution with an average $\delta\bar{f}_{q1} = -0.7$ kHz and standard deviation $\sigma = 0.5$ kHz.

Compared to state-of-the-art conventional flip-chip architectures based on coplanar waveguide architectures,[32] the isolation presented here is several orders of magnitude larger. Compared to similar architectures based on 3D-integrated floating chips in enclosures,[20] the isolation is at least comparable or one order of magnitude larger on average. This proves the effective screening of microwave signals across the enclosures, even while capacitive extenders between the enclosures are present and while the qubits are operated on resonance.

The effective transverse coupling strength g_{13}^{eff} between qubits 1 and 3 can be tuned by adapting the coupler detuning $\Delta f_c = f_c - f_{q1}$. To illustrate this, we show the measured g_{13}^{eff} in Fig. 4, which are obtained from two-tone spectroscopic measurements of avoided level splitting between qubits 1 and 3 for different coupler detunings (see the supplementary material). By applying a Schrieffer–Wolff transformation (SWT) to the coupled three-qubit array, we obtain an effective two-qubit model.[33,34] The SWT can be calculated numerically without approximation as explained in Ref. 33 and analytically using second-order perturbation, as detailed in the supplementary material. The continuous and dashed lines in Fig. 4 show fits of the SWT model to the measured g_{13}^{eff} using two parameters: the effective qubit-coupler $C_{12} = C_{23} \approx 0.2$ fF and direct qubit-qubit $C_{13} \approx 5$ aF coupling capacitances, which are given by the combination of capacitive extenders and shunting capacitances via ground [cf. Fig. 1(g)]. The individual qubit and coupler parameters are obtained from separate fits of their flux-dependent spectra[26] and summarized in the supplementary material. As expected, perturbation theory fails to predict the level splitting close to resonance, whereas the numerical results capture the tunability of the effective qubit–qubit coupling correctly.

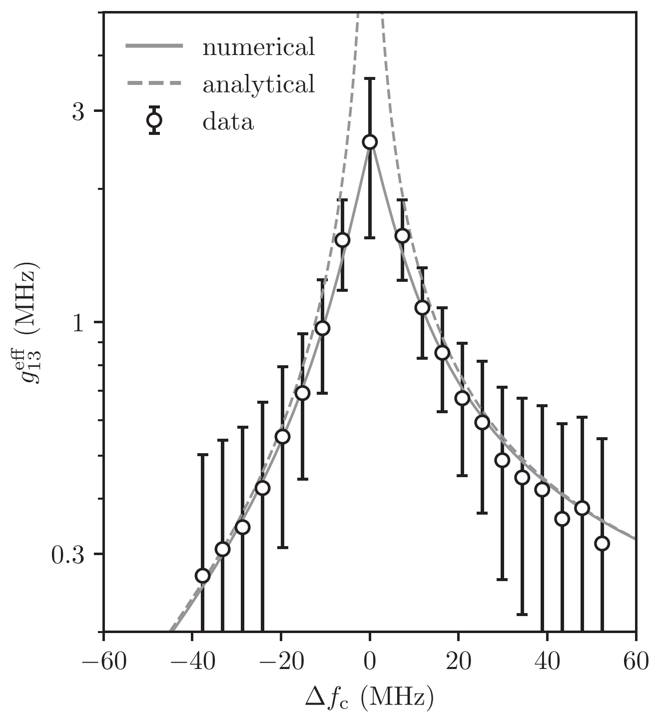

FIG. 4. Effective qubit–qubit coupling strength g_{13}^{eff} vs coupler detuning Δf_c. The data points show the measured coupling strength between q1 and q3 that are operated on resonance ($f_{q1} = f_{q3} = 3.689$ GHz) for different coupler detunings Δf_c. The errorbars represent the spectroscopic linewidth of the f_{q1}-transition used to measure the level splittings. The numerical (continuous) and analytical (dashed) theoretical curves correspond to an effective two-qubit model obtained using a Schrieffer–Wolff transformation, as detailed in the supplementary material.

The coupling strength $g_{13}^{\max} = 2.5\,\text{MHz}$ is maximal on resonance, confirming the measured qubit population swap frequency $f_{\text{SWAP}} \approx 10\,\text{MHz} = 4g_{13}^{\max}$, as detailed in the supplementary material. At the coupler sweet spot, which corresponds to a detuning of $\Delta f_c = -252\,\text{MHz}$, we measure a residual $g_{13}^{\text{eff}} = 50\,\text{kHz}$, corresponding to an ON/OFF ratio of 50 (see the supplementary material). In future experiments, the ON/OFF ratio can be optimized by designing the coupling capacitors C_{12} and C_{23} in such a way that the direct charge interaction between qubits 1 and 3, represented by a parasitic C_{13}, cancels with the one mediated by the coupler, similarly to Ref. 35.

In summary, we have demonstrated a linear array of three coupled flux qubits, each on a dedicated chip in a separate microwave enclosure, which ensures low microwave crosstalk between the outermost enclosures, below $-60\,\text{dB}$. We leverage this isolation and operate the qubits on resonance, using the center qubit as flux-tunable coupler. As a result, the architecture provides strong isolation while offering tunable coupling at the same time. In addition, the system is fully modular and allows for the substitution and reassembly of individual circuit parts. In the future, this architecture can be used to implement two-qubit gates on resonant qubits by using the coupler off-resonantly[35–39] or to investigate novel gate schemes including the coupler degree of freedom. The *one qubit one enclosure* concept presented here is directly scalable in two dimensions (see the supplementary material) and could potentially be miniaturized using micromachining techniques.[20,40,41]

See the supplementary material for more details on the capacitive coupling between the chips including corresponding finite-element simulations, the fabrication procedure, the readout and single qubit gate fidelity, the power calibration used to calculate the dephasing rate γ_m, the avoided level crossings between the qubits from which we extract the effective qubit–qubit coupling g_{13}^{eff}, the Schrieffer–Wolff transformation used to predict g_{13}^{eff}, the qubit spectra and parameters, the population transfer between the qubits, and the scaling of the architecture in two dimensions.

We are grateful to L. Radtke and S. Diewald for technical assistance. This project was financed by the European Commission via project FET-Open AVaQus, GA 899561. M. S., P. P., N. G., and T. R. acknowledge partial funding from the German Ministry of Education and Research (BMBF) within the project GEQCOS (FKZ: 13N15683). N. Z. acknowledges funding from the Deutsche Forschungsgemeinschaft (DFG—German Research Foundation) (Project No. 450396347) (GeHoldeQED). G. J. acknowledges support from the "la Caixa" Foundation (ID 100010434) via fellowship code LCF/BQ/DR22/11950032. M. P. acknowledges funding from European Union NextGenerationEU/PRTR project Consolidación Investigadora CNS2022-136025. Facilities use was supported by the KIT Nanostructure Service Laboratory. We acknowledge the measurement software framework qKit.

AUTHOR DECLARATIONS

Conflict of Interest

The authors have no conflicts to disclose.

Author Contributions

Soeren Ihssen and Simon Geisert contributed equally to this work.

Soeren Ihssen: Conceptualization (equal); Data curation (equal); Formal analysis (equal); Investigation (equal); Methodology (equal); Resources (equal); Software (equal); Validation (equal); Visualization (equal); Writing – original draft (equal); Writing – review & editing (equal). **Simon Geisert:** Conceptualization (equal); Data curation (equal); Formal analysis (equal); Investigation (equal); Methodology (equal); Resources (equal); Software (equal); Validation (equal); Visualization (equal); Writing – original draft (equal); Writing – review & editing (equal). **Gabriel Jauma:** Formal analysis (equal); Investigation (equal); Methodology (equal); Software (equal); Validation (equal); Visualization (equal); Writing – original draft (equal); Writing – review & editing (equal). **Patrick Winkel:** Conceptualization (equal); Methodology (equal); Resources (equal); Supervision (equal); Validation (equal); Writing – review & editing (equal). **Martin Spiecker:** Conceptualization (equal); Formal analysis (equal); Methodology (equal); Resources (equal); Software (equal); Validation (equal); Writing – review & editing (equal). **Nicolas Zapata:** Data curation (equal); Resources (equal); Writing – review & editing (equal). **Nicolas Gosling:** Data curation (equal); Methodology (equal); Software (equal); Writing – review & editing (equal). **Patrick Paluch:** Methodology (equal); Resources (equal); Writing – review & editing (equal). **Manuel Pino:** Supervision (equal); Writing – review & editing (equal). **Thomas Reisinger:** Resources (equal); Supervision (equal); Writing – review & editing (equal). **Wolfgang Wernsdorfer:** Resources (equal); Supervision (equal); Writing – review & editing (equal). **Juan Jose Garcia-Ripoll:** Supervision (equal); Writing – review & editing (equal). **Ioan M. Pop:** Conceptualization (equal); Data curation (equal); Formal analysis (equal); Funding acquisition (equal); Investigation (equal); Methodology (equal); Project administration (equal); Resources (equal); Software (equal); Supervision (equal); Validation (equal); Visualization (equal); Writing – original draft (equal); Writing – review & editing (equal).

DATA AVAILABILITY

The data that support the findings of this study are available from the corresponding author upon reasonable request.

REFERENCES

[1]A. Blais, A. L. Grimsmo, S. M. Girvin, and A. Wallraff, "Circuit quantum electrodynamics," Rev. Mod. Phys. **93**, 025005 (2021).

[2]F. Arute, K. Arya, R. Babbush, D. Bacon, J. C. Bardin, R. Barends, R. Biswas, S. Boixo, F. G. S. L. Brandao, D. A. Buell, B. Burkett, Y. Chen, Z. Chen, B. Chiaro, R. Collins, W. Courtney, A. Dunsworth, E. Farhi, B. Foxen, A. Fowler, C. Gidney, M. Giustina, R. Graff, K. Guerin, S. Habegger, M. P. Harrigan, M. J. Hartmann, A. Ho, M. Hoffmann, T. Huang, T. S. Humble, S. V. Isakov, E. Jeffrey, Z. Jiang, D. Kafri, K. Kechedzhi, J. Kelly, P. V. Klimov, S. Knysh, A. Korotkov, F. Kostritsa, D. Landhuis, M. Lindmark, E. Lucero, D. Lyakh, S. Mandrà, J. R. McClean, M. McEwen, A. Megrant, X. Mi, K. Michielsen, M. Mohseni, J. Mutus, O. Naaman, M. Neeley, C. Neill, M. Y. Niu, E. Ostby, A. Petukhov, J. C. Platt, C. Quintana, E. G. Rieffel, P. Roushan, N. C. Rubin, D. Sank, K. J. Satzinger, V. Smelyanskiy, K. J. Sung, M. D. Trevithick, A. Vainsencher, B. Villalonga, T. White, Z. J. Yao, P. Yeh, A. Zalcman, H. Neven, and J. M. Martinis, "Quantum supremacy using a programmable superconducting processor," Nature **574**, 505 (2019).

[3]Y. Wu, W.-S. Bao, S. Cao, F. Chen, M.-C. Chen, X. Chen, T.-H. Chung, H. Deng, Y. Du, D. Fan, M. Gong, C. Guo, C. Guo, S. Guo, L. Han, L. Hong, H.-L. Huang, Y.-H. Huo, L. Li, N. Li, S. Li, Y. Li, F. Liang, C. Lin, J. Lin, H. Qian, D. Qiao, H. Rong, H. Su, L. Sun, L. Wang, S. Wang, D. Wu, Y. Xu, K. Yan, W. Yang, Y. Yang, Y. Ye, J. Yin, C. Ying, J. Yu, C. Zha, C. Zhang, H. Zhang, K.

Zhang, Y. Zhang, H. Zhao, Y. Zhao, L. Zhou, Q. Zhu, C.-Y. Lu, C.-Z. Peng, X. Zhu, and J.-W. Pan, "Strong quantum computational advantage using a superconducting quantum processor," Phys. Rev. Lett. **127**, 180501 (2021).
[4]S. Krinner, N. Lacroix, A. Remm, A. Di Paolo, E. Genois, C. Leroux, C. Hellings, S. Lazar, F. Swiadek, J. Herrmann, G. J. Norris, C. K. Andersen, M. Müller, A. Blais, C. Eichler, and A. Wallraff, "Realizing repeated quantum error correction in a distance-three surface code," Nature **605**, 669 (2022).
[5]J. F. Marques, B. M. Varbanov, M. S. Moreira, H. Ali, N. Muthusubramanian, C. Zachariadis, F. Battistel, M. Beekman, N. Haider, W. Vlothuizen, A. Bruno, B. M. Terhal, and L. DiCarlo, "Logical-qubit operations in an error-detecting surface code," Nat. Phys. **18**, 80 (2022).
[6]Google Quantum AI, "Suppressing quantum errors by scaling a surface code logical qubit," Nature **614**, 676 (2023).
[7]Y. Kim, C. J. Wood, T. J. Yoder, S. T. Merkel, J. M. Gambetta, K. Temme, and A. Kandala, "Scalable error mitigation for noisy quantum circuits produces competitive expectation values," Nat. Phys. **19**, 752 (2023).
[8]Google Quantum AI and Collaborators, "Quantum error correction below the surface code threshold," Nature **638**, 920 (2024).
[9]L. Cardani, F. Valenti, N. Casali, G. Catelani, T. Charpentier, M. Clemenza, I. Colantoni, A. Cruciani, G. D'Imperio, L. Gironi, L. Grünhaupt, D. Gusenkova, F. Henriques, M. Lagoin, M. Martinez, G. Pettinari, C. Rusconi, O. Sander, C. Tomei, A. V. Ustinov, M. Weber, W. Wernsdorfer, M. Vignati, S. Pirro, and I. M. Pop, "Reducing the impact of radioactivity on quantum circuits in a deep-underground facility," Nat. Commun. **12**(1), 2733 (2021).
[10]M. McEwen, L. Faoro, K. Arya, A. Dunsworth, T. Huang, S. Kim, B. Burkett, A. Fowler, F. Arute, J. C. Bardin, A. Bengtsson, A. Bilmes, B. B. Buckley, N. Bushnell, Z. Chen, R. Collins, S. Demura, A. R. Derk, C. Erickson, M. Giustina, S. D. Harrington, S. Hong, E. Jeffrey, J. Kelly, P. V. Klimov, F. Kostritsa, P. Laptev, A. Locharla, X. Mi, K. C. Miao, S. Montazeri, J. Mutus, O. Naaman, M. Neeley, C. Neill, A. Opremcak, C. Quintana, N. Redd, P. Roushan, D. Sank, K. J. Satzinger, V. Shvarts, T. White, Z. J. Yao, P. Yeh, J. Yoo, Y. Chen, V. Smelyanskiy, J. M. Martinis, H. Neven, A. Megrant, L. Ioffe, and R. Barends, "Resolving catastrophic error bursts from cosmic rays in large arrays of superconducting qubits," Nat. Phys. **18**, 107 (2022).
[11]C. D. Wilen, S. Abdullah, N. A. Kurinsky, C. Stanford, L. Cardani, G. D'Imperio, C. Tomei, L. Faoro, L. B. Ioffe, C. H. Liu, A. Opremcak, B. G. Christensen, J. L. DuBois, and R. McDermott, "Correlated charge noise and relaxation errors in superconducting qubits," Nature **594**, 369 (2021).
[12]T. Thorbeck, A. Eddins, I. Lauer, D. T. McClure, and M. Carroll, "Two-level-system dynamics in a superconducting qubit due to background ionizing radiation," PRX Quantum **4**, 020356 (2023).
[13]E. Yelton, C. P. Larson, V. Iaia, K. Dodge, G. La Magna, P. G. Baity, I. V. Pechenezhskiy, R. McDermott, N. A. Kurinsky, G. Catelani, and B. L. T. Plourde, "Modeling phonon-mediated quasiparticle poisoning in superconducting qubit arrays," Phys. Rev. B **110**, 024519 (2024).
[14]N. Janzen, M. Kononenko, S. Ren, and A. Lupascu, "Aluminum air bridges for superconducting quantum devices realized using a single-step electron-beam lithography process," Appl. Phys. Lett. **121**, 094001 (2022).
[15]N. T. Bronn, V. P. Adiga, S. B. Olivadese, X. Wu, J. M. Chow, and D. P. Pappas, "High coherence plane breaking packaging for superconducting qubits," Quantum Sci. Technol. **3**, 024007 (2018).
[16]J. L. Mallek, D. R. W. Yost, D. Rosenberg, J. L. Yoder, G. Calusine, M. T. Cook, R. Das, A. L. Day, E. B. Golden, D. K. Kim, J. Knecht, B. M. Niedzielski, M. Schwartz, A. Sevi, C. Stull, W. Woods, A. J. Kerman, and W. D. Oliver, "Fabrication of superconducting through-silicon vias," arXiv:2103.08536 (2021).
[17]M. Mollenhauer, A. Irfan, X. Cao, S. Mandal, and W. Pfaff, "A high-efficiency plug-and-play superconducting qubit network," arXiv:2407.16743 (2024).
[18]K. S. Chou, T. Shemma, H. McCarrick, T.-C. Chien, J. D. Teoh, P. Winkel, A. Anderson, J. Chen, J. C. Curtis, S. J. de Graaf, J. W. O. Garmon, B. Gudlewski, W. D. Kalfus, T. Keen, N. Khedkar, C. U. Lei, G. Liu, P. Lu, Y. Lu, A. Maiti, L. Mastalli-Kelly, N. Mehta, S. O. Mundhada, A. Narla, T. Noh, T. Tsunoda, S. H. Xue, J. O. Yuan, L. Frunzio, J. Aumentado, S. Puri, S. M. Girvin, S. H. Moseley, and R. J. Schoelkopf, "A superconducting dual-rail cavity qubit with erasure-detected logical measurements," Nat. Phys. **20**, 1454 (2024).
[19]A. Copetudo, C. Y. Fontaine, F. Valadares, and Y. Y. Gao, "Shaping photons: Quantum information processing with bosonic cQED," Appl. Phys. Lett. **124**, 080502 (2024).
[20]P. A. Spring, S. Cao, T. Tsunoda, G. Campanaro, S. Fasciati, J. Wills, M. Bakr, V. Chidambaram, B. Shteynas, L. Carpenter, P. Gow, J. Gates, B. Vlastakis, and P. J. Leek, "High coherence and low cross-talk in a tileable 3D integrated superconducting circuit architecture," Sci. Adv. **8**, eabl6698 (2022).
[21]S. Kosen, H.-X. Li, M. Rommel, D. Shiri, C. Warren, L. Grönberg, J. Salonen, T. Abad, J. Biznárová, M. Caputo, L. Chen, K. Grigoras, G. Johansson, A. F. Kockum, C. Križan, D. P. Lozano, G. J. Norris, A. Osman, J. Fernández-Pendás, A. Ronzani, A. F. Roudsari, S. Simbierowicz, G. Tancredi, A. Wallraff, C. Eichler, J. Govenius, and J. Bylander, "Building blocks of a flip-chip integrated superconducting quantum processor," Quantum Sci. Technol. **7**, 035018 (2022).
[22]D. R. W. Yost, M. E. Schwartz, J. Mallek, D. Rosenberg, C. Stull, J. L. Yoder, G. Calusine, M. Cook, R. Das, A. L. Day, E. B. Golden, D. K. Kim, A. Melville, B. M. Niedzielski, W. Woods, A. J. Kerman, and W. D. Oliver, "Solid-state qubits integrated with superconducting through-silicon vias," npj Quantum Inf. **6**, 59 (2020).
[23]M. Field, A. Q. Chen, B. Scharmann, E. A. Sete, F. Oruc, K. Vu, V. Kosenko, J. Y. Mutus, S. Poletto, and A. Bestwick, "Modular superconducting-qubit architecture with a multichip tunable coupler," Phys. Rev. Appl. **21**, 054063 (2024).
[24]M. Bild, M. Fadel, Y. Yang, U. von Lüpke, P. Martin, A. Bruno, and Y. Chu, "Schrödinger cat states of a 16-microgram mechanical oscillator," Science **380**, 274 (2023).
[25]C. R. Conner, A. Bienfait, H.-S. Chang, M.-H. Chou, É. Dumur, J. Grebel, G. A. Peairs, R. G. Povey, H. Yan, Y. P. Zhong, and A. N. Cleland, "Superconducting qubits in a flip-chip architecture," Appl. Phys. Lett. **118**, 232602 (2021).
[26]S. Geisert, S. Ihssen, P. Winkel, M. Spiecker, M. Fechant, P. Paluch, N. Gosling, N. Zapata, S. Günzler, D. Rieger, D. Bénâtre, T. Reisinger, W. Wernsdorfer, and I. M. Pop, "Pure kinetic inductance coupling for cQED with flux qubits," Appl. Phys. Lett. **125**, 064002 (2024).
[27]M. D. Reed, B. R. Johnson, A. A. Houck, L. DiCarlo, J. M. Chow, D. I. Schuster, L. Frunzio, and R. J. Schoelkopf, "Fast reset and suppressing spontaneous emission of a superconducting qubit," Appl. Phys. Lett. **96**, 203110 (2010).
[28]E. A. Sete, J. M. Martinis, and A. N. Korotkov, "Quantum theory of a bandpass purcell filter for qubit readout," Phys. Rev. A **92**, 012325 (2015).
[29]Magnetic shielding, see https://www.quantum-machines.co/products/qcage/ for "QCage: QPU chip carrier" (last accessed July 15, 2024).
[30]P. Winkel, I. Takmakov, D. Rieger, L. Planat, W. Hasch-Guichard, L. Grünhaupt, N. Maleeva, F. Foroughi, F. Henriques, K. Borisov, J. Ferrero, A. V. Ustinov, W. Wernsdorfer, N. Roch, and I. M. Pop, "Nondegenerate parametric amplifiers based on dispersion-engineered josephson-junction arrays," Phys. Rev. Appl. **13**, 024015 (2020).
[31]J. Gambetta, A. Blais, D. I. Schuster, A. Wallraff, L. Frunzio, J. Majer, M. H. Devoret, S. M. Girvin, and R. J. Schoelkopf, "Qubit-photon interactions in a cavity: Measurement-induced dephasing and number splitting," Phys. Rev. A **74**, 042318 (2006).
[32]S. Kosen, H.-X. Li, M. Rommel, R. Rehammar, M. Caputo, L. Grönberg, J. Fernández-Pendás, A. F. Kockum, J. Biznárová, L. Chen, C. Križan, A. Nylander, A. Osman, A. F. Roudsari, D. Shiri, G. Tancredi, J. Govenius, and J. Bylander, "Signal crosstalk in a flip-chip quantum processor," PRX Quantum **5**, 030350 (2024).
[33]M. Hita-Pérez, G. Jaumà, M. Pino, and J. J. García-Ripoll, "Three-Josephson junctions flux qubit couplings," Appl. Phys. Lett. **119**, 222601 (2021).
[34]G. Consani and P. A. Warburton, "Effective Hamiltonians for interacting superconducting qubits: Local basis reduction and the Schrieffer–Wolff transformation," New J. Phys. **22**, 053040 (2020).
[35]Y. Sung, L. Ding, J. Braumüller, A. Vepsäläinen, B. Kannan, M. Kjaergaard, A. Greene, G. O. Samach, C. McNally, D. Kim, A. Melville, B. M. Niedzielski, M. E. Schwartz, J. L. Yoder, T. P. Orlando, S. Gustavsson, and W. D. Oliver, "Realization of high-fidelity CZ and ZZ-free iSWAP gates with a tunable coupler," Phys. Rev. X **11**, 021058 (2021).
[36]Y. Chen, C. Neill, P. Roushan, N. Leung, M. Fang, R. Barends, J. Kelly, B. Campbell, Z. Chen, B. Chiaro, A. Dunsworth, E. Jeffrey, A. Megrant, J. Y. Mutus, P. J. J. O'Malley, C. M. Quintana, D. Sank, A. Vainsencher, J. Wenner, T. C. White, M. R. Geller, A. N. Cleland, and J. M. Martinis, "Qubit architecture with high coherence and fast tunable coupling," Phys. Rev. Lett. **113**, 220502 (2014).

[37] D. C. McKay, S. Filipp, A. Mezzacapo, E. Magesan, J. M. Chow, and J. M. Gambetta, "Universal gate for fixed-frequency qubits via a tunable bus," Phys. Rev. Appl. **6**, 064007 (2016).

[38] S. J. Weber, G. O. Samach, D. Hover, S. Gustavsson, D. K. Kim, A. Melville, D. Rosenberg, A. P. Sears, F. Yan, J. L. Yoder, W. D. Oliver, and A. J. Kerman, "Coherent coupled qubits for quantum annealing," Phys. Rev. Appl. **8**, 014004 (2017).

[39] I. N. Moskalenko, I. A. Simakov, N. N. Abramov, A. A. Grigorev, D. O. Moskalev, A. A. Pishchimova, N. S. Smirnov, E. V. Zikiy, I. A. Rodionov, and I. S. Besedin, "High fidelity two-qubit gates on fluxoniums using a tunable coupler," npj Quantum Inf. **8**(1), 130 (2022).

[40] T. Brecht, Y. Chu, C. Axline, W. Pfaff, J. Z. Blumoff, K. Chou, L. Krayzman, L. Frunzio, and R. J. Schoelkopf, "Micromachined integrated quantum circuit containing a superconducting qubit," Phys. Rev. Appl. **7**, 044018 (2017).

[41] D. Rosenberg, S. J. Weber, D. Conway, D.-R. W. Yost, J. Mallek, and G. Calusine, "Solid-state qubits: 3D integration and packaging," IEEE Microwave Mag. **21**, 72 (2020).